Thermodynamically stable lithium silicides and germanides from density functional theory calculations

Andrew J. Morris,[1,*] C. P. Grey,[2] and Chris J. Pickard[3]

[1]*Theory of Condensed Matter Group, Cavendish Laboratory, University of Cambridge, J. J. Thomson Avenue, Cambridge CB3 0HE, United Kingdom*

[2]*Department of Chemistry, University of Cambridge, Lensfield Road, Cambridge CB2 1EW, United Kingdom*

[3]*Department of Physics and Astronomy, University College London, Gower Street, London WC1E 6BT, United Kingdom*

(Received 25 February 2014; revised manuscript received 1 August 2014; published 21 August 2014)

High-throughput density functional theory (DFT) calculations have been performed on the Li-Si and Li-Ge systems. Lithiated Si and Ge, including their metastable phases, play an important technological role as Li-ion battery (LIB) anodes. The calculations comprise structural optimizations on crystal structures obtained by swapping atomic species to Li-Si and Li-Ge from the X-Y structures in the International Crystal Structure Database, where $X = \{\text{Li, Na, K, Rb, Cs}\}$ and $Y = \{\text{Si, Ge, Sn, Pb}\}$. To complement this at various Li-Si and Li-Ge stoichiometries, *ab initio* random structure searching (AIRSS) was also performed. Between the ground-state stoichiometries, including the recently found $Li_{17}Si_4$ phase, the average voltages were calculated, indicating that germanium may be a safer alternative to silicon anodes in LIB due to its higher lithium insertion voltage. Calculations predict high-density Li_1Si_1 and Li_1Ge_1 $P4/mmm$ layered phases which become the ground states above 2.5 and 5 GPa, respectively, and reveal silicon and germanium's propensity to form dumbbells in the Li_xSi, $x = 2.33$–3.25, stoichiometry range. DFT predicts the stability of the $Li_{11}Ge_6$ $Cmmm$, $Li_{12}Ge_7$ $Pnma$, and Li_7Ge_3 $P32_12$ phases and several new Li-Ge compounds, with stoichiometries Li_5Ge_2, $Li_{13}Ge_5$, Li_8Ge_3 and $Li_{13}Ge_4$.

DOI: 10.1103/PhysRevB.90.054111 PACS number(s): 61.05.−a, 82.47.Aa

I. INTRODUCTION

Lithium-ion batteries (LIBs) are the secondary (rechargeable) battery of choice for portable electronic devices due to their high specific energy (energy per unit weight) and energy density (energy per unit volume). LIBs have the highest capacity of all the commercially available battery technologies and are now being deployed in hybrid and all-electric vehicles [1]. There is substantial interest in enhancing the capacity of LIBs, driven by the economic and environmental advantages of increasing the range of electric vehicles, and enabling longer-life portable electronic devices.

Lithium intercalated graphite is the standard LIB negative-electrode material due to its good rate capability and cyclability, but demand for even higher performance LIBs has motivated the investigation of other materials. Silicon is an attractive alternative since it has 10 times the gravimetric and volumetric capacity of graphite (calculated from the initial mass and volume of silicon), but unlike graphite, silicon undergoes structural changes on lithiation [2–4]. The negative electrode may be studied using a half cell containing lithium and silicon. The term "anode" applies to the negative electrode during LIB discharge only, so to avoid confusion we refer to *lithiation* and *delithiation* of the silicon half cell, which correspond to charging and discharging the LIB, respectively. The first lithiation of the cell at room temperature involves the conversion of crystalline silicon (c-Si) into an amorphous lithium silicide phase (a-Li_ySi) [5]. The onset of amorphization depends on the lithiation rate and has been measured at $y \approx 0.3$ in micron-sized (325 mesh) silicon clusters after irreversible solid-electrolyte interphase (SEI) formation has been taken into account [6,7]. Below a discharge voltage of 50 mV the a-Li_ySi crystallizes to form a metastable $Li_{15}Si_4$ phase which may become nonstoichiometric, $Li_{15+\delta}Si_4$, at deep discharge [6]. However, at temperatures above 100 °C it is possible to form the most lithiated crystalline phase, $Li_{21}Si_5$, electrochemically [8]. Full lithiation of silicon leads to a drastic volume expansion of 270%–280% [9], which generates considerable mechanical stress. Hysteresis in the capacity-voltage profile occurs due to a combination of mechanical stress and different reactions taking different structural pathways on lithiation and delithiation. The microscopic mechanisms underlying these phenomena are still not entirely clear [9]. a-Li_ySi has been studied *in situ* using nuclear magnetic resonance (NMR) [6], x-ray diffraction (XRD) [10,11], and electron-energy-loss spectroscopy (EELS) [12]. These studies along with *ex situ* NMR and pair-distribution function (PDF) studies of XRD data suggest that silicon forms small clusters and isolated atoms during lithiation. The clusters that form only break apart into isolated silicon atoms at the end of the lithiation process (below 80 mV). [13] One proposed solution to reduce the stress and microcracks [14] caused by lithiation is to use nanostructured silicon, e.g., nanowires (SiNW) [15,16], or nanocomposites [17] (see also the review of silicon-based materials by Liang *et al.* [18]).

Many of the disordered structures that form during lithiation can be approximated by the Li-Si ground-state and metastable crystalline phases. For instance, the crystalline phases have been used as a first step in understanding charge transfer [19] and average lithiation voltages [20]. To gain insight into the possible types of silicon clusters present and their environments in a-Li_ySi, various crystalline phases have been investigated and categorized using NMR [6,21] and *ab initio* theoretical techniques [19,22–24]. These c-Li-Si phases have previously been well categorized using density functional theory (DFT) [19,22,23,25]; however, new insights into the most lithiated phases and the ability to synthesize Li_1Si_1

*ajm255@cam.ac.uk

through ball milling have suggested that the system is far from fully understood. The most recent phase diagram of the Li-Si system shows, in ascending lithium content order, *c*-Si, Li_1Si_1, $Li_{12}Si_7$, Li_7Si_3, $Li_{13}Si_4$, $Li_{15}Si_4$, $Li_{22}Si_5$, and β-Li [26]. Additionally, investigations by Zeilinger and coworkers have presented a high-temperature $Li_{4.11}Si$ phase [24,27] and suggested $Li_{17}Si_4$ as the correct stoichiometry of $Li_{21}Si_5/Li_{22}Si_5$.

Germanium is another choice of anode for LIB with a theoretical capacity of 1568 mAh g^{-1}, some 5 times greater than carbon. It has also been proposed as a protective coating for SiNW anodes [28,29]. Germanium's lithium diffusivity at room temperature is 400 times greater than that of silicon [30]; however, it is scarcer and, consequently, more expensive. First-principles studies comparing lithiation of amorphous germanium and silicon show lithium diffusivity is less concentration dependent than in silicon [31]. However, about the Li-Ge phase diagram, much less is known. In increasing order of lithium content, the following stable phases have all been proposed: Li_7Ge_{12} [32], Li_1Ge_1 [33,34], $Li_{12}Ge_7$ [32], $Li_{11}Ge_6$ [35], Li_9Ge_4 [36–38], Li_7Ge_3 [32,37], Li_7Ge_2 [38,39], $Li_{15}Ge_4$ [37,38,40,41], $Li_{17}Ge_4$ [42], and $Li_{22}Ge_5$ [37,38,43]. More crystalline phases occur during electrochemical lithiation of germanium than during electrochemical lithiation of silicon; XRD and high-resolution transmission electron microscopy measurements show that during lithiation of germanium at room temperature, the Li-Ge system progresses through Li_9Ge_4, Li_7Ge_2, and a mixture of $Li_{15}Ge_4$ and $Li_{22}Ge_5$ [38].

In this paper we use atomic species swapping along with random-structure-searching techniques, described in Sec. II, to predict ground-state and metastable crystal structures of the Li-Si and Li-Ge systems. In Sec. III our approach to calculating average voltages is discussed, and Secs. IV and V describe the DFT-predicted phases of Li-Si and Li-Ge, respectively. In the Li-Si system we predict a high-density Li_1Si_1 phase with $P4/mmm$ symmetry and discuss the tendency for silicon to form dumbbells within the lithium silicides. We then turn our attention to Li-Ge, which has not been analyzed using these computational search methods before, and predict the new structures, Li_5Ge_2, $Li_{13}Ge_5$, Li_8Ge_3, and $Li_{13}Ge_4$. The average voltages for the Li-Si and Li-Ge systems are presented, including the $Li_{17}Si_4$ and Li_1Si_1 phases. The conclusions of the simulations are given in Sec. VI.

II. METHODS

Ab initio random structure searching (AIRSS) has been successful in predicting the ground-state structures of high-pressure phases of matter [44,45]. More recently, it has also been applied to the Li-P system [46] and defects in technologically relevant ceramics [47,48], semiconductors [49,50], and LIBs [51,52]. Since, in an AIRSS calculation, each random starting configuration is independent of the others, the search algorithm is trivially parallelizable, making high-throughput computation straightforward. AIRSS searches were performed for stoichiometries Li_xSi_y and Li_xGe_y, where $x,y = 1$–8. Atoms were placed in a simulation cell commensurate with one of the 230 space groups chosen randomly. Initial cell volumes were between $\pm 50\%$ of an appropriate target volume chosen by considering phases from the International Crystallographic Structure Database (ICSD). Due to their unphysical nature, cells where atoms were closer than 1 Å apart were rejected. All initial cells were transformed into ones with cell angles between 60° and 120°.

Relaxations were performed using the stoichiometric crystal structures of Li-Si, Li-Ge, Li-Sn, Li-Pb, Na-Si, Na-Ge, Na-Sn, Na-Pb, K-Si, K-Ge, K-Sn, and K-Pb. First, the structures were obtained from the ICSD. Second, for each structure the anions were replaced with Li, and the cations were replaced with {Si,Ge}. The structures were relaxed to local energy minima using forces and stresses calculated by DFT. Via this technique, other stoichiometries beyond those searched using AIRSS are also sampled.

Calculations were performed using the plane-wave CASTEP DFT code [53]. The Perdew-Burke-Ernzerhof (PBE) exchange-correlation functional was used with Vanderbilt "ultrasoft" pseudopotentials. The Li-Si system required a basis set containing plane waves with energies of up to 400 eV and a Monkhorst-Pack (MP) grid corresponding to a Brillouin zone (BZ) sampling grid finer than $2\pi \times 0.05$ Å^{-1}. The Li-Ge system required a 600-eV plane-wave cutoff with harder pseudopotentials and a BZ sampling finer than $2\pi \times 0.03$ Å^{-1}.

We define the formation energy per atom of a compound Li_mX_n, where $X = \{Si,Ge\}$, as

$$E_f/A = \frac{E(Li_nX_m) - n\mu_{Li} - m\mu_X}{n+m}, \quad (1)$$

where $E(Li_nX_m)$ is the total DFT energy of a given structure, Li_nX_m, and μ_{Li} and μ_X are the chemical potentials of atomic species Li and X in their ground-state elemental structure, i.e., Li in the $P63/mmc$ space group and Si and Ge in the (diamond) $Fd\bar{3}m$ space group.

To compare the stabilities of different stoichiometries we use the Maxwell construction [54,55]. The second law of thermodynamics demands that the (free) energy per atom is a convex function of the relative concentrations of the atoms. For each structure that we generate, we plot its formation energy per atom E_f/A versus its fractional concentration of lithium in the compound, where

$$C_{Li} = \frac{n}{n+m} \quad (2)$$

and, as above, n and m are the number of atoms of Li and X in the compound, respectively. Then, starting at $(C_{Li}, E_f/A) = (0,0)$ and ending at $(1,0)$, we join together the lowest possible points with tie-lines, while maintaining a convex function (i.e., each tie-line has a gradient equal to or larger than the last). Hence we obtain a "convex hull" between the chemical potentials, which reveals the stable 0 K structures at the vertices of the tie-lines. For a further discussion of convex hulls and their application to hydrogen/lithium defects in silicon we refer the reader to our previous publication [51].

III. VOLTAGES

We calculate average voltages in an LIB anode using DFT total energies by assuming that all the displaced charge is due to Li and that the reaction proceeds sequentially through the phases on the tie-lines of the convex hull; that is, it is a succession of two-phase reactions [56]. The electrical energy

obtained from the two-phase reaction $A(x_1) \rightarrow B(x_2)$, whose structures contain x_1 and x_2 lithium atoms, respectively, is

$$\Delta E_{A\rightarrow B} = -\frac{1}{e}\int_{q_1}^{q_2} V(q)dq = -\int_{x_1}^{x_2} \mu(x) - \mu_{\mathrm{Li}}\, dx, \quad (3)$$

where we have replaced the voltage $V(q)$ with the differences in chemical potential between the anode, $\mu(x)$, and bulk lithium, μ_{Li}, multiplied by the electronic charge e. We have made the substitution, $dq = e\,dx$ by assuming that all displaced charge q is due to lithium displacement. Since the reaction is in two phases, the solution of the integral is

$$\Delta E_{A\rightarrow B} = -\{G_{\mathrm{A}} - G_{\mathrm{B}} - \Delta x G_{\mathrm{Li}}\}, \quad (4)$$

which equals the negative of the Gibbs free-energy change of the reaction ΔG, where G_{A}, G_{B}, and G_{Li} are the Gibbs free energies of A, B, and bulk lithium, respectively.

The Gibbs free-energy change can be resolved into a number of terms,

$$\Delta G = \Delta E + P\Delta V - T\Delta S, \quad (5)$$

where ΔE is the total electronic energy and P, ΔV, T, and ΔS are the pressure, change in volume, thermodynamic temperature, and change in entropy, respectively. Due to the difficulty in calculating ΔG we make the approximation, previously applied to the Li-Si system, that $\Delta G \approx \Delta E$ since ΔE is of the order of a few electron volts, $P\Delta V \approx 10^{-5}$ eV, and $T\Delta S \approx 0.06$ eV at 425 °C [20,57,58]. The average voltage $\overline{V}_{A\rightarrow B}$ is given (in eV) by

$$\overline{V}_{A\rightarrow B} = -\frac{\Delta G}{\Delta x}, \quad (6)$$

where Δx is the change in the number of Li atoms. Therefore, the average voltage of a two-phase process relative to lithium metal is

$$\overline{V}_{A\rightarrow B} = -\frac{\{E_B/X - E_A/X - \mu_{\mathrm{Li}}\Delta x\}}{\Delta x}, \quad (7)$$

where E_1/X and E_2/X are the total electronic energies per $X = \{\mathrm{Si/Ge}\}$ atom.

IV. RESULTS: LITHIUM SILICIDE

We find on the convex hull (shown Fig. 1), in increasing lithium content order, diamond-structure $Fd\bar{3}m$ c-Si; the $I4_1/a$ $\mathrm{Li_1Si_1}$ phase [59,60], which has recently been synthesized at ambient pressure [61] and is discussed in Sec. IV A; the $Pnma$ $\mathrm{Li_{12}Si_7}$ phase [62], which contains silicon five-membered rings and four-membered stars, which have been studied using NMR [21]; the $\mathrm{Li_7Si_3}$ and $\mathrm{Li_5Si_2}$ phases with $P3_212$ and $R\bar{3}m$ symmetries, respectively, which are discussed further in Sec. IV B; the $Pbam$ $\mathrm{Li_{13}Si_4}$ phase; the metastable $I4\bar{3}d$ $\mathrm{Li_{15}Si_4}$; and the $\mathrm{Li_{17}Si_4}$ $F\bar{4}3m$ symmetry phase, which is discussed further in Sec. IV C.

For $\mathrm{Li_{15}Si_4}$, Mulliken analysis yields a charge of $0.15|e|$ and $-0.57|e|$ for Li and Si, respectively, which is in agreement with Bader analysis that Li is a cation [19] and contrary to the reports that Li is anionic [63].

The average voltage was calculated between all adjacent pairs of stable Li-Si phases on the convex hull, including both the $\mathrm{Li_{17}Si_4}$ phase and the $\mathrm{Li_1Si_1}$ phase recently synthesized at ambient pressure. Voltages were obtained from the DFT total energies, as described in Sec. III, and referenced to lithium metal. The potential composition curve is presented in Fig. 2 and is in agreement with previous experimental and theoretical work.

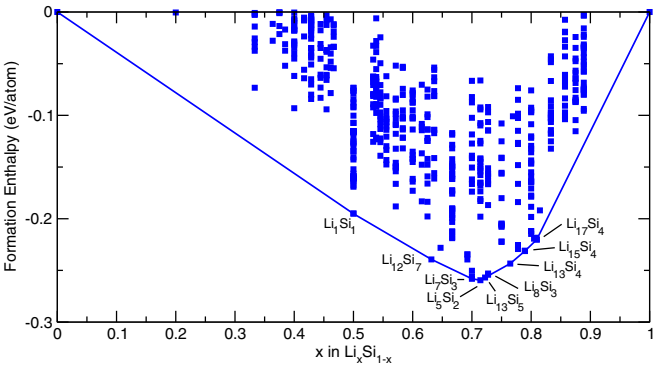

FIG. 1. (Color online) Formation enthalpy per atom vs the fractional lithium concentration of a Li-Si compound (blue boxes). The tie-line (blue line) shows the convex hull obtained by joining together the globally stable structures predicted by DFT. Between the species swapping technique and AIRSS we recover the known stable phases, $\mathrm{Li_1Si_1}$, $\mathrm{Li_{12}Si_7}$, $\mathrm{Li_7Si_3}$, $\mathrm{Li_{13}Si_4}$, $\mathrm{Li_{15}Si_4}$, and $\mathrm{Li_{17}Si_4}$. The searches also find the $\mathrm{Li_5Si_2}$ phase predicted by Tipton *et al.* [58], and low-lying metastable phases with stoichiometries $\mathrm{Li_8Si_3}$ and $\mathrm{Li_{13}Si_5}$ are also predicted.

A. $\mathrm{Li_1Si_1}$ layered structures

We find a set of structures with $\mathrm{Li_1Si_1}$ stoichiometry, listed in Table I, that are all within ∼0.1 eV/f.u. of the ground state. The DFT ground state at 0 GPa is an $I4_1/a$ phase comprising a threefold-coordinated silicon network hosting lithium tetrahedra similar to the $\{4\mathrm{Li},\ V\}$ *Zintl defect* in silicon [52]. Recently, the $I4_1/a$ phase has been synthesized via ball milling and has been shown to be stable under ambient conditions [61]. Mulliken analysis yields a charge of $0.34|e|$

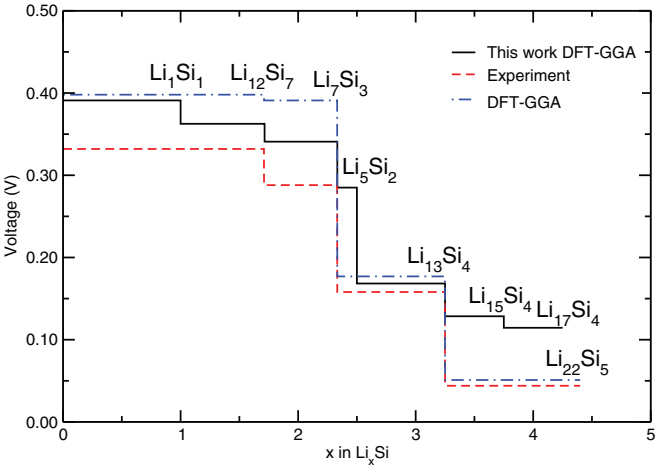

FIG. 2. (Color online) Potential-composition curves of stable structures found on the convex hull in Fig. 1 (black line) compared to experiment at 415 °C (red dashed line) [3] and previous DFT-GGA calculations (blue dot-dashed line) [20].

TABLE I. Low-energy Li_1Si_1 metastable phases. The structures are shown in Fig. 3 with formation energy E_f per formula unit relative to the energy of the ground states. We calculate that $P4/mmm$ is the most stable above 2.5 GPa.

E_f (eV/f.u.)	Symmetry	Volume (Å^3/f.u.)	Description
0.00	$I4_1/a$	31.3	Li tetrahedra in a threefold-coordinated Si network
0.05	$R\bar{3}$	33.1	Distorted Li octahedra threefold-coordinated Si network
0.07	$P4/mmm$	27.8	Flat Si sheets comprising four-member rings
0.07	$P\bar{1}$	31.7	Buckled Si sheets comprising eight- and four-member rings
0.07	$P\bar{3}m1$	34.1	Li intercalated silicene
0.08	$P2/m$	28.1	Li_1Sn_1-like 2.39 Å dumbbells and isolated atoms
0.11	$I4_1/amd$	28.1	Isostructural with Li_1Ge_1 high-pressure phase

for each Li and $-0.34|e|$ for each Si, establishing Li as cationic, contrary to a previous analysis [60].

DFT predicts a novel $P4/mmm$ phase with a formation energy of 0.07 eV/f.u. at 0 GPa. It is a layered structure comprising a two-dimensional (nontetrahedrally) fourfold-coordinated silicon lattice with lithium intercalated between the silicon sheets. Since the silicon is fourfold coordinated, it gains less of the lithium's charge than in the $I4_1/a$ phase; Mulliken analysis shows lithium atoms each donate $0.22|e|$. Our calculations show the Li_1Si_1 system undergoes a phase transition from the $I4_1/a$ phase to the $P4/mmm$ phase at 2.5 GPa.

The $I4_1/amd$ phase is isostructural to its Li_1Ge_1 analog. Li_1Ge_1 $I4_1/amd$ is stable at high pressure [34]; however, Li_1Si_1 $I4_1/amd$ is not globally stable over the pressure range we studied (between 0 and 10 GPa).

The $P\bar{3}m1$ phase contains six-member rings of threefold-coordinated silicon atoms in layered sheets (see Fig. 3). The silicon network is isostructural to silicene, a silicon analog of graphene. We calculate that silicene and a phase based on the $P4/mmm$ silicon network are 0.63 and 0.89 eV/f.u., respectively, above the $Fd\bar{3}m$ ground state. When lithiated, both layered structures are only 0.07 eV above the ($I4_1/a$) ground state. Given the interest in silicene, our layered

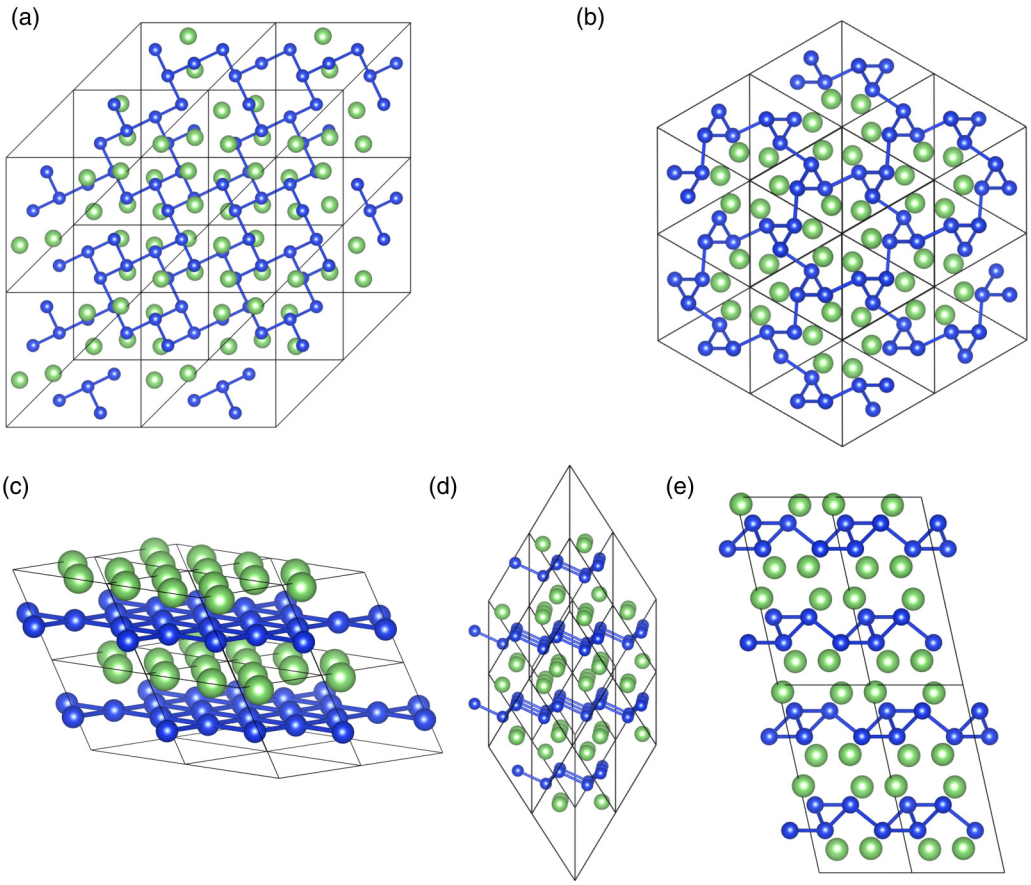

FIG. 3. (Color online) Low-energy Li_1Si_1 phases detailed in Table I with (a) $I4_1/a$, (b) $R\bar{3}$, (c) $P4/mmm$, (d) $P\bar{3}m1$, and (e) $P\bar{1}$ symmetries. DFT predicts the $P4/mmm$ phase is stable above 2.5 GPa.

compounds might provide an alternative route to layered silicon.

B. Li_7Si_3 and Li_5Si_2

Lithium's position in the crystal lattice can be difficult to establish due to its low XRD scattering factor. Furthermore, Li_7Si_3 has partially occupied lattice sites [64], making it difficult to model using DFT. Its structure may be represented as a supercell of $R\bar{3}m$ Li_5Si_2 in which lithium atoms have been removed from certain lattice sites [65]. By choosing different combinations of lithium sites in the supercell, models of Li_7Si_3 can be produced with $P\bar{3}m1$, $C2/m$, Cm, and $P3_212$ symmetries. The latter, labeled "#2" by Dahn *et al.* [19], is found on the convex hull.

It is unsurprising that at 0 K, DFT also predicts that the $R\bar{3}m$ Li_5Si_2 phase will be stable since it contains entirely occupied lithium sites. Tipton *et al.* also found this phase to be stable using DFT [58].

C. Most lithiated phases

The most lithiated stable Li-Si phase has been the subject of debate. XRD measurements predict that $Li_{21}Si_5$ [66] is stable at room temperature and $Li_{22}Si_5$ is stable at 415 °C [3]. Previous DFT calculations predict $Li_{21}Si_5$ is the stabler phase, even after the inclusion of temperature dependence using the harmonic approximation [19]. The combined AIRSS/species-swapping technique predicts $Li_{21}Si_5$ and $Li_{22}Si_5$ are locally stable but above the convex hull. The $Li_{17}Si_4$ phase is on the convex hull, and it has the same crystal structure as $F\bar{4}3m$ $Li_{17}Pb_4$, as discovered independently by Zeilinger *et al.* [24]. Zeilinger *et al.* also predict a $Li_{4.11}Si$ high-temperature phase, which they model using $Li_{16}Si_4$ and $Li_{16.5}Si_4$ phases. We include Zeilinger *et al.*'s models in Fig. 1, although DFT predicts that they are not on the tie-line [67].

D. Repeating units: Silicon dumbbells

We also find $R\bar{3}m$ Li_8Si_3 and $P\bar{3}m1$ $Li_{13}Si_4$ phases close above the tie-line. They belong to the set of structures in the range $Li_7Si_3 \rightarrow Li_{13}Si_5$ which all contain silicon dumbbells. The dumbbells are aligned in parallel with various numbers of collinear lithium atoms between them forming one-dimensional repeating sequences (see Table II). The one-dimensional linear repeating chains are thus packed alongside each other, realizing the three-dimensional structure. For example, since Li_7Si_3 comprises (5 × Li + Si-Si) and (4× Li + Si-Si) sequences in a ratio of 2:1, it is equivalent to the Li_5Si_2 phase with lithium vacancies. Li_5Si_2 comprises sequences of atoms with the repeating unit (5 × Li + Si-Si), and Li_8Si_3 is similar, but with atoms in a (4 × Li + Si + 4 × Li + Si-Si) repeating unit; it is isostructural with a Li_8Pb_3 phase [68]. The $Li_{13}Si_5$ phase is isostructural with the $Li_{13}Sn_5$ phase [69] and has two different repeating units, (5 × Li + Si) and (4 × Li + Si-Si), in a ratio of 1:2.

Finally, in $Li_{13}Si_4$ the one-dimensional columnar structure does not exist, but Si-Si dumbbells and Si isolated atoms remain in a ratio of 1:1. At higher lithium concentrations, $Li_{15}Si_4$ forms, in which all silicon dumbbells are broken, and only isolated Si atoms remain. The propensity for silicon dumbbells to form over a wide range of stoichiometries and total energies implies that silicon dumbbells form on lithiation of silicon in a LIB anode.

V. RESULTS: LITHIUM GERMANIDE

In order of lithium content, the following Li-Ge phases have all been proposed (Table III): Li_7Ge_{12}, Li_1Ge_1, $Li_{12}Ge_7$, $Li_{11}Ge_6$, Li_9Ge_4, Li_7Ge_3, Li_7Ge_2, $Li_{15}Ge_4$, $Li_{17}Ge_4$, and $Li_{22}Ge_5$. Below we compare in detail the known phases to the results of the DFT searches.

Li_7Ge_{12} is the only reported phase with a ratio of Li/Ge less than 1. It has two symmetries associated with it, originally $Pmn2_1$ [32,72], which was later disputed [70], and, more recently, $P2/n$ [73]. Four of its lithium lattice sites are 50% occupied. We model its structure in a periodic lattice using a simulation cell containing 28 Li and 48 Ge sites. The fractionally occupied sites can be filled in a variety of ways: all sites can be filled, giving rise to a crystal symmetry $P2/c$; one site ($P1$) can be filled in four different ways (all degenerate); two sites can be filled six ways (Pc, $P2$, or $P\bar{1}$), with each symmetry being doubly degenerate; three sites ($P1$) can be filled four ways (all degenerate); and all sites can be left empty ($P2/c$). A convex hull of their single-point energies shows that the Pc version is the most stable; hence we use this throughout the rest of the calculations. Although not on the Li-Ge convex hull (see Fig. 4), this Pc predicted phase is close above it.

Li_1Ge_1 has an $I4_1/a$ [79] ground state and a $I4_1/amd$ [80] high-pressure form. DFT predicts $I4_1/amd$ and a new layered $P4/mmm$ phase ∼0.012 eV/f.u. and ∼0.020 eV/f.u. above the $I4_1/a$ ground state, respectively (Table IV). The $P4/mmm$ phase is isostructural with the Li-Si phase discussed in Sec. IV A. DFT predicts that the system undergoes a phase transition from the $I4_1/amd$ phase to the $P4/mmm$ phase at 5 GPa.

Grüttner *et al.* mentioned a $Li_{12}Ge_7$ phase isotypic with the corresponding $Li_{12}Si_7$ phase [32] in a very brief report but did not present any further data to support its discovery. DFT also predicts a $Li_{12}Ge_7$ $Pnma$ phase near the tie-line.

$Li_{11}Ge_6$ was synthesized by Frank and Müller [35] with a molecular volume of 172.3 cm^3 mol^{-1}. Nesper *et al.* [74] claim that the phase is actually Li_8MgGe_6, suggesting that since Li_8MgGe_6 has a molecular volume of 166.5 cm^3 mol^{-1},

TABLE II. Structures in the stoichiometry range Li_xSi, $x = 2.33$–2.60, exhibit parallel silicon dumbbells situated in one-dimensional linear columns containing variable numbers of silicon dumbbells and isolated lithium and silicon atoms. The columns are packed together, realizing the three-dimensional structure. The repeating units in each column are represented in parentheses, and silicon dumbbells are indicated by Si-Si. For example, a structure comprising columns containing a repeating unit of five lithium atoms followed by a silicon dumbbell is represented as (5 × Li + Si-Si).

Stoichiometry	Constituent columns
Li_7Si_3	2 × (5 × Li + Si-Si) and (4 × Li + Si-Si)
Li_5Si_2	(5 × Li + Si-Si)
$Li_{13}Si_5$	(5 × Li + Si) and 2 × (4× Li + Si-Si)
Li_8Si_3	(4 × Li + Si + 4 × Li + Si-Si)

TABLE III. Experimental and predicted phases of the Li_xGe system. Sangster and Pelton's work was invaluable for an overview of the field [70]. A single asterisk (*) indicates first metastable above tie-line. Two asterisks (**) indicate second metastable above tie-line.

Experimental symmetry	x	Stoichiometry	Predicted symmetry
$Fd\bar{3}m$[a]	0.000	Ge	$Fd\bar{3}m$
$Pmn2_1$,[b] $P2/n$[c]	0.580	Li_7Ge_{12}	Pc^*
$I4_1/a$[d], $I4_1/amd$*[e]	1.000	Li_1Ge_1	$I4_1/a$, $I4_1/amd^*$, $P4/mmm^{**}$
$Pnma$[f]	1.710	$Li_{12}Ge_7$	$Pnma^*$
$Cmcm$[g]	1.83	$Li_{11}Ge_6$	$Cmcm^*$
$Cmcm$[h,i,j]	2.25	Li_9Ge_4	$Cmcm^*$
$P32_12$[f], $R\bar{3}m$[i]	2.33	Li_7Ge_3	$P32_12$, $P21/m^*$
	2.50	Li_5Ge_2	$R\bar{3}m^*$
	2.60	$Li_{13}Ge_5$	$P\bar{3}m1$
	2.67	Li_8Ge_3	$R\bar{3}m$
?[k]	3.20	$Li_{16}Ge_5$	
	3.25	$Li_{13}Ge_4$	$Pbam^*$
$Cmmm$[j,l]	3.50	Li_7Ge_2	$P\bar{3}m1^*$, $Cmmm^{**}$
$I\bar{4}3d$[i,j,m]	3.75	$Li_{15}Ge_4$	$I\bar{4}3d$
$F\bar{4}3m$[n]	4.20	$Li_{17}Ge_4$	$F\bar{4}3m$
$F\bar{4}3m$[j,o,p]	4.25	$Li_{22}Ge_5$	$F\bar{4}3m^*$
$P6_3/mmc$[q]		αLi	$P6_3/mmc$

[a]Hull [71].
[b]Very brief summaries are given by Grüttner *et al.* [32,72].
[c]Kiefer and Fässler [73].
[d]Menges *et al.* [33].
[e]Evers *et al.* [34].
[f]Reported in the abstract by Grüttner *et al.* [32].
[g]First found by Frank and Müller [35]; Nesper *et al.* [74] suggested it is actually Li_8MgGe_6.
[h]Hopf *et al.* [36].
[i]Jain *et al.* [37].
[j]Yoon *et al.* [38].
[k]Pell finds Li_3Ge_1 [75]. See Sangster and Pelton [70] and discussion therein. St. John *et al.* report that they have found the Li_3Ge_1 reported earlier as $Li_{16}Ge_5$ [77].
[l]Hopf *et al.* [39].
[m]Gladyshevskii and Kripyakevich [40] and Johnson *et al.* [41].
[n]Goward *et al.* [42].
[o]Gladyshevskii *et al.* [43].
[p]Reported by Jain *et al.* [37] as $Li_{21.1875}Ge_5$.
[q]Barrett [78].

it is unlikely that $Li_{11}Ge_6$ could have two more atoms per formula unit [76]. DFT also finds a $Li_{11}Ge_6$ $Cmcm$ phase slightly above the tie-line with a volume of 286.26 Å^3/f.u., which corresponds to a molecular volume of 172.4 cm^3 mol^{-1}. Hence it seems entirely possible to us that $Li_{11}Ge_6$ $Cmcm$ was synthesized by Frank and Müller as initially proposed.

Li_9Ge_4 in the $Cmcm$ symmetry group has been made electrochemically and from high-temperature fusion [37,38,70], but all of our calculations show it well above the tie-line, favoring disproportion into a $P32_12$ Li_7Ge_3 phase.

Li_7Ge_3 with $P32_12$ symmetry was first mentioned by Ref. [32], but no supporting information was given. Jain *et al.* found an unknown phase that they suggested was Li_7Ge_3 by fitting the diffraction data to $R\bar{3}m$ symmetry [37]. Hence we suggest that Jain *et al.* synthesized either the Li_5Ge_2 or, indeed,

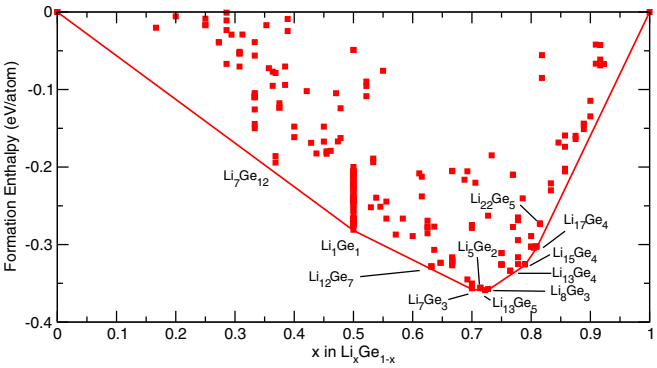

FIG. 4. (Color online) Li-Ge binary composition diagram. The red squares indicate the formation enthalpy of a structure. The red line is the tie-line indicating the stable structures at 0 K predicted by DFT.

the Li_8Ge_3 phase, with DFT predicting that both phases have $R\bar{3}m$ symmetry. Li_5Ge_2 is above the tie-line, and $Li_{13}Ge_5$ and Li_8Ge_3 are all stable, although to the best of our knowledge they have not previously been presented in the literature. This may be due to thermal effects; see the discussion of similar arguments for Li_5Si_2 in Sec. IV B. $Li_{16}Ge_5$ was predicted by St. John *et al.* [77] during electrochemical studies. They presented no crystal structure, nor is there any prototype structure of {Li/Na}{Si/Ge/Sn/Pb} with this stoichiometry. DFT predicts a $Li_{13}Ge_4$ $Pbam$ phase, isostructural with the $Li_{13}Si_4$ phase, which is slightly above the tie-line and has a Li:Si ratio similar to that of $Li_{16}Ge_5$. Recently, preliminary results by Jung *et al.* [81] have produced electrochemically new phases in the $Li_{2.33}Ge$-$Li_{3.5}Ge$ range whose x-ray PDFs match at least one of our predicted phases. A more complete investigation will be presented in a future publication.

The Li_7Ge_2 phase with $Cmmm$ symmetry can be made electrochemically and by annealing from high-temperature melt [38,70]. DFT-GGA predicts the $P\bar{3}m1$ phase is above the tie-line and is 0.08 eV/f.u more stable than the $Cmmm$ phase. This discrepancy remains after using harder pseudopotentials and either the local-density-approximation (LDA) exchange-correlation functional and the Heyd-Scuseria-Ernzerhof 2006 (HSE06) hybrid functional [82]. A more complete investigation into this will be presented in a future publication.

We find the well-known $Li_{15}Ge_4$ stoichiometry $I\bar{4}3d$ phase to be stable [37,38,40,41]. The most lithiated phase has been a matter of debate in all Li group 4 compounds including germanium. Its stoichiometry was reported as $Li_{22}Ge_5$ with $F23$ symmetry [43] due to its similarity to $Li_{22}Pb_4$ [83]. More recently, Goward *et al.* [42] studied this family of structures and showed that for the Ge, Sn, and Pb compounds the correct stoichiometry is $Li_{17}Ge_4$ with $F\bar{4}3m$ symmetry. $F\bar{4}3m$ symmetry $Li_{21}Ge_5$, $Li_{22}Ge_5$, and $Li_{17}Ge_4$ are found by DFT, all at local energy minima. However, $Li_{17}Ge_4$ is on the tie-line. Zeilinger *et al.* [27] also predict a $Li_{4.10}Ge$ phase analogous to the $Li_{4.11}Si$ phase. We use the same model structures as in the $Li_{4.11}Si$ phase for our DFT calculations. These are above the tie-line, as is expected for a high-temperature phase.

The Li-Ge system has an inclination to forming Ge-Ge dumbbells analogous to that in Li-Si, as discussed in Sec. IV D.

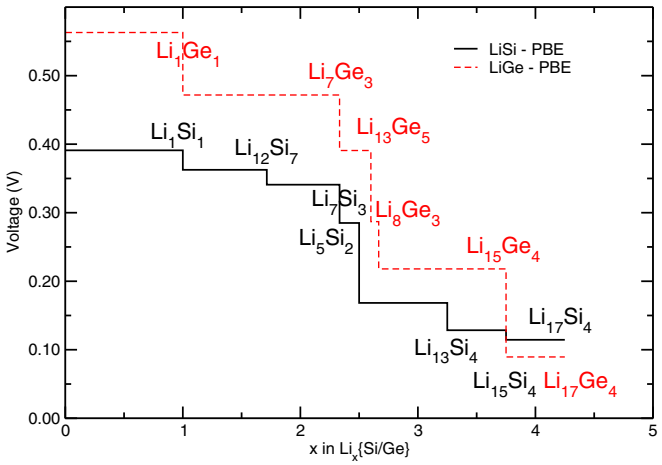

FIG. 5. (Color online) Potential-composition curves of stable structure found on the Li-Si and Li-Ge convex hull diagrams. The Li-Ge results are at a higher average voltage.

VI. DISCUSSION

Crystal structures of the Li-Si and Li-Ge systems have been presented, found using both AIRSS searches and atomic species swapping of ICSD structures. Below we discuss the structures at local minima of the DFT potential energy surface which reside on, or close to, the convex hull since they are the most likely to be thermally accessible at room temperature. These structures serve as a model for the clustering and bonding behavior of electrochemically lithiated silicon and germanium [16].

The Li-Si system was used to validate our method: DFT finds all of the known phases as local energy minima, including independently uncovering the $Li_{17}Si_4$ phase. For the Li-Ge system, DFT finds Li_5Ge_2, Li_8Ge_3, $Li_{13}Ge_5$, and $Li_{13}Ge_4$ are locally stable, and to the best of our knowledge, these have not been presented in the literature before. DFT predicts that Li_7Ge_{12} and $Li_{11}Ge_6$ are local energy minima; the former has Pc symmetry, and the latter has $Cmcm$. It was reported that $Li_{11}Ge_6$ may be produced from a high-temperature melt [35], but this has been disputed [74]. Also at local energy minima are the $Li_{12}Ge_7$ $Pnma$ and Li_7Ge_3 $P32_12$ phases, which were suggested by Grüttner *et al.* [32], who did not present the crystal structure. An unknown phase was found by heating ball-milled Li-Ge; its XRD pattern fits an Li_7Ge_3 phase with $R\bar{3}m$ symmetry. Since DFT and Grüttner *et al.* both predict that Li_7Ge_3 has $P32_12$ symmetry, we propose that the unknown phase may be either the Li_5Ge_2 phase or the Li_8Ge_3 phase, both of which have a stoichiometry similar to Li_7Ge_3 and are predicted by DFT to have $R\bar{3}m$ symmetry.

Overall, the Li-Si and Li-Ge convex hull diagrams are qualitatively similar; however, Li-Ge has a deeper hull than Li-Si by -0.11 eV/atom, and as a consequence, the average voltages for Li-Ge are higher by $\sim$30% (Fig. 5). For the Li-Si and Li-Ge structures on the tie-lines, the average voltages were calculated relative to lithium metal. This included the recently proposed $Li_{17}Si_4$ phase and the Li_1Si_1 phase which has recently been synthesized through ball-milling. To the best of our knowledge these have not been included in previous potential-composition curves. The average voltages are in good agreement with both previous calculations and experiment. They are higher in Li-Ge than in Li-Si, implying that germanium has a lower energy density than silicon. However, the higher insertion voltage is safer during lithiation, reducing the chance of lithium plating, which can result in dendrites short-circuiting the cell. Lithium in germanium also has higher diffusivity than that in silicon.

A LIB does not necessarily have time to equilibrate thermodynamically over large length scales [6]. The ability to generate a wide range of locally stable low-energy structures above the ground state allows us to visualize the types of clusters which form in the LIB during cycling. Over a lithiation range of Li_xSi, $x = 2.33$–3.25, we found that the structures exhibit Si-Si dumbbells. At higher lithiation all of the silicon dumbbells break up, and the crystalline $Li_{15}Si_4$ phase forms. Since these dumbbells were seen in both ground-state and metastable phases, it seems likely that they will exist in LIB anodes, probably in a lower-symmetry solid solution. Furthermore we find the analogous dumbbell-containing structures in the Li-Ge system.

Dumbbells break at lower lithium concentrations in Li-Ge than in Li-Si. The Li_7Si_3, Li_5Si_2, and $Li_{13}Si_4$ structures that DFT predicts are on the convex hull in the range $x = 2.33$ to 3.25 all contain dumbbells. The $Li_{15}Ge_4$ phase (comprising only isolated Ge) forms at a more convex point than $Li_{15}Si_4$ and hence is relatively more stable than its Li-Si analog; as a consequence, unlike $Li_{13}Si_4$, $Li_{13}Ge_4$ (composed of one Ge dumbbell per four Ge atoms) is not on the tie-line. The $Li_{13}Ge_5$ and Li_8Ge_3 phases both contain isolated atoms as well as dumbbells, with ratios of dumbbells to total Ge atoms of 2:5 and 1:3 respectively. Unlike their Li-Si counterparts, $Li_{13}Ge_5$ and Li_8Ge_3 are on the hull, displacing the Li_5Ge_2 phase, which comprises only dumbbells. Hence isolated group IV atoms begin to form between $x = 2.33$ and 2.66 in Li-Ge but not until between $x = 2.50$ and 3.25 in Li-Si. The lengths of the dumbbells in the dumbbell phases (see Fig. 6) follow the same trends

TABLE IV. Low-energy Li_1Ge_1 metastable phases, with formation energy E_f per formula unit relative to that of the energy of the ground state. The structures are isotypic of those found in Li_1Si_1, as shown in Table I and Fig. 3. DFT predicts that the $P4/mmm$ phase is the most stable above 5 GPa.

E_f (eV/f.u.)	Symmetry	Volume (Å^3/f.u.)	Description
0.00	$I4_1/a$	35.1	Li tetrahedra in a threefold-coordinated Ge network
0.01	$I41/amd$	32.2	Known high-pressure phase
0.02	$P4/mmm$	31.9	Flat Ge sheets, four-member rings
0.03	$R\bar{3}$	36.8	Distorted Li octahedra in a threefold-coordinated Ge network
0.04	$P2/m$	32.1	Isostructural with the corresponding Li_1Sn_1 phase

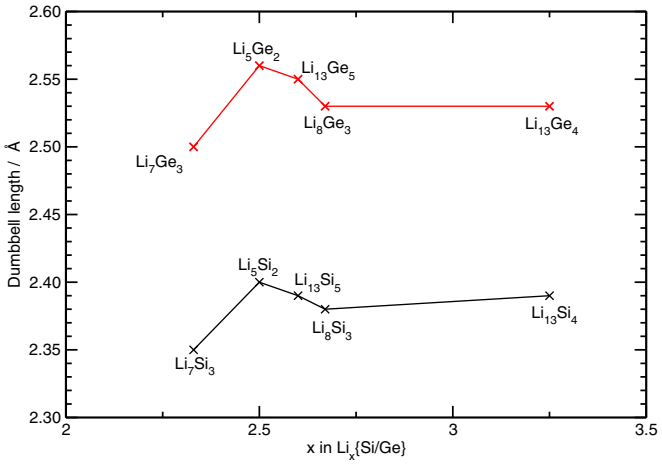

FIG. 6. (Color online) Lengths of dumbbells in Li-Si- and Li-Ge-containing compounds. Germanium dumbbells are longer than those of silicon, but the lengths follow the same trend on lithiation.

in Li-Si as in Li-Ge. However, germanium has a higher Pauling electronegativity (2.01) than silicon (1.90); hence it is able to satisfy the "octet rule" through obtaining a greater proportion of charge from the lithium, resulting in weaker covalent bonds.

Li_1Si_1 was previously only synthesizable at high pressure but has recently been synthesized by highly energetic ball milling, remotivating interest in the high-pressure phases. AIRSS searches predict a selection of higher-energy Li_1Si_1 and Li_1Ge_1 phases. At lower pressures three-dimensional threefold-coordinated silicon/germanium networks were prevalent. However, at higher densities, both silicon and germanium exhibited a $P4/mmm$ structure comprising flat sheets of fourfold-coordinated silicon and germanium atoms, respectively. These became the most stable phases of Li_1Si_1 and Li_1Ge_1 at 2.5 and 5 GPa, respectively. Given the interest in silicene, our layered compounds might provide an alternative route to layered silicon.

Above we have demonstrated that the combination of both atomic species swapping the ICSD phases and AIRSS is a powerful tool for predicting the crystal structures of LIB electrode materials. A refinement to the method combines these two techniques by using results of the AIRSS searches as inputs to the species-swapping technique. For example, the low-energy structures found by AIRSS in Li_1Si_1 were reoptimized as candidate Li_1Ge_1 phases in the Li-Ge system.

Our method has only provided results of the stable and metastable structures at 0 K; of course, the effect of temperature could be included *post hoc* using phonon calculations within the harmonic approximation and beyond. Our method serves as a crucial first step in *ab initio* materials discovery and design.

ACKNOWLEDGMENTS

The authors would like to thank E. Engel for useful discussions and H. Jung, Y.-Y. Hu, and P. K. Allan for sharing their preliminary results and useful discussions. A.J.M. acknowledges the support from the Winton Programme for the Physics of Sustainability. This work was supported by the Engineering and Physical Sciences Research Council (EPSRC) of the United Kingdom. Computational resources were provided by the University College London Research Computing service and the Cambridge High Performance Computing service.

[1] S. Chu and A. Majumdar, Nature (London) **488**, 294 (2012).
[2] S. Lai, J. Electrochem. Soc. **123**, 1196 (1976).
[3] C. J. Wen and R. A. Huggins, J. Solid State Chem. **37**, 271 (1981).
[4] W. J. Weydanz, M. Wohlfahrt-Mehrens, and R. A. Huggins, J. Power Sources **81-82**, 237 (1999).
[5] J. P. Maranchi, A. F. Hepp, and P. N. Kumta, Electrochem. Solid State Lett. **6**, A198 (2003); P. Limthongkul, Y.-I. Jang, N. J. Dudney, and Y.-M. Chiang, J. Power Sources **119–121**, 604 (2003); Acta Mater. **51**, 1103 (2003).
[6] B. Key, R. Bhattacharyya, M. Morcrette, V. Seznéc, J.-M. Tarascon, and C. P. Grey, J. Am. Chem. Soc. **131**, 9239 (2009).
[7] J. Li and J. R. Dahn, J. Electrochem. Soc. **154**, A156 (2007).
[8] J. Y. Kwon, J. H. Ryu, and S. M. Oh, Electrochem. Acta **55**, 8051 (2010).
[9] M. N. Obrovac and L. J. Krause, J. Electrochem. Soc. **154**, A103 (2007).
[10] T. D. Hatchard and J. R. Dahn, J. Electrochem. Soc. **151**, A838 (2004).
[11] M. N. Obrovac and L. Christensen, Electrochem. Solid State Lett. **7**, A93 (2004).
[12] Y.-M. Kang, S.-B. Suh, and Y.-S. Kim, Inorg. Chem. **48**, 11631 (2009).
[13] B. Key, M. Morcrette, J.-M. Tarascon, and C. P. Grey, J. Am. Chem. Soc. **133**, 503 (2011).
[14] Y. S. Choi, M. Pharr, C. S. Kang, S.-B. Son, S. C. Kim, K.-B. Kim, H. Roh, and S.-H. Lee, K. H. Oh, and J. J. Vlassak, J. Power Sources **265**, 160 (2014).
[15] C. K. Chan, H. Peng, G. Liu, K. McIlwrath, X. F. Zhang, R. A. Huggins, and Y. Cui, Nat. Nanotechnol. **3**, 31 (2008).
[16] K. Ogata, E. Salager, C. J. Kerr, A. E. Fraser, C. Ducati, A. J. Morris, S. Hofmann, and C. P. Grey, Nat. Commun. **5**, 3217 (2014).
[17] D. M. Piper, J. H. Woo, S.-B. Son, S. C. Kim, K. H. Oh, and S.-H. Lee, Adv. Mater. **26**, 3520 (2014).
[18] B. Liang, Y. Liu, and Y. Xu, J. Power Sources **267**, 469 (2014).
[19] V. L. Chevrier, J. Zwanziger, and J. R. Dahn, J. Alloy Compd. **496**, 25 (2010).
[20] V. L. Chevrier, J. W. Zwanziger, and J. R. Dahn, Can. J. Phys. **87**, 625 (2009).
[21] T. K.-J. Köster, E. Salager, A. J. Morris, B. Key, V. Seznec, M. Morcrette, C. J. Pickard, and C. P. Grey, Angew. Chem. Int. Ed. **123**, 12799 (2011).
[22] V. L. Chevrier and J. R. Dahn, J. Electrochem. Soc. **157**, A392 (2010).

[23] V. L. Chevrier and J. R. Dahn, J. Electrochem. Soc. **156**, A454 (2009).

[24] M. Zeilinger, I. M. Kurylyshyn, U. Häussermann, and T. F. Fässler, Chem. Mater. **25**, 1960 (2013).

[25] M. H. Braga, A. Dębski, and W. Gąsior, Journal of Alloys and Compounds (2014), doi:10.1016/j.jallcom.2014.06.212.

[26] H. Okamoto, J. Phase Equilib. Diffus. **30**, 118 (2009).

[27] M. Zeilinger, I. M. Kurylyshyn, U. Häussermann, and T. F. Fässler, Chem. Mater. **25**, 4623 (2013).

[28] T. Song, H. Cheng, H. Choi, J.-H. Lee, H. Han, D. H. Lee, D. S. Yoo, M.-S. Kwon, J.-M. Choi, S. G. Doo, H. Chang, J. Xiao, Y. Huang, W. I. Park, Y.-C. Chuang, H. Kim, J.-A. Rogers, and U. Paik, ACS Nano **6**, 303 (2012).

[29] Y. Yu, C. Yue, S. Sun, W. Lin, H. Su, B. Xu, J. Li, S. Wu, J. Li, and J. Kang, ACS Appl. Mater. Interfaces **6**, 5884 (2014).

[30] C.-M. Park, J.-H. Kim, H. Kim, and H.-J. Sohn, Chem. Soc. Rev. **39**, 3115 (2010).

[31] C.-Y. Chou and G. S. Hwang, J. Power Sources **263**, 252 (2014).

[32] A. Grüttner, R. Nesper, and H. G. von Schnering, Acta. Crystallog. A **37**, C161 (1981), http://journals.iucr.org/a/issues/1981/a1/00/a43079/a43079.pdf.

[33] E. Menges, V. Hopf, H. Schäfer, and A. Weiss, Z. Naturforsch. B **24**, 1351 (1969).

[34] J. Evers, G. Oehlinger, G. Sextl, and H.-O. Becker, Angew. Chem. Int. Ed. **26**, 76 (1987).

[35] U. Frank and W. Müller, Z. Naturforsch. B **30**, 313 (1975).

[36] V. Hopf, H. Schäfer, and A. Weiss, Z. Naturforsch. B **25**, 653 (1970).

[37] A. Jain, E. Kawasako, H. Miyaoka, T. Ma, S. Isobe, T. Ichikawa, and Y. Kojima, J. Phys. Chem. C **117**, 5650 (2013).

[38] S. Yoon, C.-M. Park, and H.-J. Sohn, Electrochem. Solid State Lett. **11**, A42 (2008).

[39] V. Hopf, W. Müller, and H. Schäfer, Z. Naturforsch. B **27**, 1157 (1972).

[40] E. L. Gladyshevskii and P. I. Kripyakevich, Sov. Phys. Crystallogr. **5**, 549 (1961).

[41] Q. Johnson, G. S. Smith, and D. Wood, Acta Crystallogr. **18**, 131 (1965).

[42] G. R. Goward, N. J. Taylor, D. C. S. Souza, and L. F. Nazar, J. Alloys Compd. **329**, 82 (2001).

[43] E. L. Gladyshevskii, G. I. Oleksiv, and P. I. Kripyakevich, Sov. Phys. Crystallogr. **9**, 269 (1964).

[44] C. J. Pickard and R. J. Needs, Phys. Rev. Lett. **97**, 045504 (2006).

[45] C. J. Pickard and R. J. Needs, J. Phys.: Condens. Matter **23**, 053201 (2011).

[46] A. S. Ivanov, A. J. Morris, K. V. Bozhenko, C. J. Pickard, and A. I. Boldyrev, Angew. Chem. Int. Ed. **51**, 8330 (2012).

[47] J. Mulroue, A. J. Morris, and D. M. Duffy, Phys. Rev. B. **84**, 094118 (2011).

[48] J. Mulroue, M. Watkins, A. J. Morris, and D. Duffy, J. Nucl. Mater. **437**, 261 (2013).

[49] A. J. Morris, C. J. Pickard, and R. J. Needs, Phys. Rev. B **78**, 184102 (2008).

[50] A. J. Morris, C. J. Pickard, and R. J. Needs, Phys. Rev. B **80**, 144112 (2009).

[51] A. J. Morris, C. P. Grey, R. J. Needs, and C. J. Pickard, Phys. Rev. B **84**, 224106 (2011).

[52] A. J. Morris, R. J. Needs, E. Salager, C. P. Grey, and C. J. Pickard, Phys. Rev. B **87**, 174108 (2013).

[53] S. J. Clark, M. D. Segall, C. J. Pickard, P. J. Hasnip, M. I. J. Probert, K. Refson, and M. C. Payne, Z. Kristallogr. **220**, 567 (2005).

[54] J. W. Gibbs, Trans. Conn. Acad. Arts Sci. **2**, 309 (1873); **2**, 382 (1873).

[55] J. C. Maxwell, *Theory of Heat* (Longmans, Green, London, 1904), pp. 195–208; *Scientific Letters and Papers of J. C. Maxwell*, edited by P. M. Harman (Cambridge University Press, Cambridge, 2002), Vol. 3, pp. 1874–1879.

[56] M. K. Aydinol, A. F. Kohan, G. Ceder, K. Cho, and J. Joannopoulos, Phys. Rev. B **56**, 1354 (1997).

[57] I. A. Courtney, J. S. Tse, O. Mao, J. Hafner, and J. R. Dahn, Phys. Rev. B **58**, 15583 (1998).

[58] W. W. Tipton, C. R. Bealing, K. Mathew, and R. G. Hennig, Phys. Rev. B **87**, 184114 (2013).

[59] L. A. Stearns, J. Gryko, J. Diefenbacher, G. K. Ramachandran, and P. F. McMillan, J. Solid State Chem. **173**, 251 (2003).

[60] Y. Kubota, M. C. S. Escaño, H. Nakanishi, and H. Kasai, J. Alloys Compd. **458**, 151 (2008).

[61] W. S. Tang, J.-N. Chotard, and R. Janot, J. Electrochem. Soc. **160**, A1232 (2013).

[62] R. Nesper, H. G. von Schnering, and J. Curda, Chem. Ber. **119**, 3576 (1986).

[63] Y. Kubota, M. C. S. Escaño, H. Nakanishi, and H. Kasai, J. Appl. Phys. **102**, 053704 (2007).

[64] H.-G. von Schnering, R. Nesper, K.-F. Tebbe, and J. Curda, Z. Metallkd. **71**, 357 (1980).

[65] I. Barvík, Czech J. Phys. B **33**, 1338 (1983).

[66] R. Nesper and H. G. von Schnering, J. Solid State Chem. **70**, 48 (1987).

[67] Since the $Li_{16.5}Si_4$ model contains partially occupied Li sites, we extended the cell in the *a* direction, fully occupying four 8*g* and two 4*c* sites before optimizing the geometry using DFT.

[68] K. Cenzual, M. N. Gelato, M. Penzo, and E. Parthe, Z. Kristallogr. **193**, 217 (1990).

[69] U. Frank and W. Müller, Z. Naturforsch. B **30**, 316 (1975).

[70] J. Sangster and A. D. Pelton, J. Phase Equilib. **18**, 289 (1997).

[71] A. W. Hull, Phys. Rev. **20**, 113 (1922).

[72] A. Grüttner, R. Nesper, and H. G. von Schnering, Agnew. Chem. Int. Ed. **21**, 912 (1982).

[73] F. Kiefer and T. F. Fässler, Solid State Sci. **13**, 636 (2011).

[74] R. Nesper, J. Curda, and H. G. von Schnering, J. Solid State Chem. **62**, 199 (1986).

[75] E. M. Pell, J. Phys. Chem. Solids **3**, 74 (1957).

[76] Confusingly, Sangster and Pelton [70] report that Nesper *et al.* [74] claim it is the Li_8MgSi_6 phase.

[77] M. R. St. John, A. J. Furgala, and A. F. Sammells, J. Electrochem. Soc. **129**, 247 (1982).

[78] C. S. Barret, Phys. Rev. **72**, 245 (1947).

[79] E. Menges. V. Hopf, H. Schaefer, and A. Weiss, Z. Naturforsch. B **27**, 313 (1975).

[80] J. Evers, G. Oehlinger, G. Sextl, and H. O. Becker, Angew. Chem. **99**, 69 (1987).

[81] H. Jung, Y.-Y. Yau, P. K. Allen, and C. P. Grey (unpublished).

[82] A. V. Krukau, O. A. Vydrov, A. F. Izmaylov, and G. E. Scuseria, J. Chem. Phys. **125**, 224106 (2006).

[83] A. Zalkin and W. J. Ramsey, J. Phys. Chem. **62**, 689 (1958).